IEEE Access
Multidisciplinary | Rapid Review | Open Access Journal

Received November 13, 2019, accepted December 18, 2019, date of publication January 10, 2020, date of current version January 24, 2020.

Digital Object Identifier 10.1109/ACCESS.2020.2965741

Experimental Testbed and Methodology for the Assessment of RTK GNSS Receivers Used in Precision Agriculture

MARCO PINI[1], GIANLUCA MARUCCO[1], GIANLUCA FALCO[1], MARIO NICOLA[1], AND WIM DE WILDE[2]
[1]LINKS Foundation, 10138 Torino, Italy
[2]Septentrio, 3001 Leuven, Belgium

Corresponding author: Marco Pini (marco.pini@linksfoundation.com)

This work was supported in part by the European GNSS Agency (GSA) under the European Union's Fundamental Elements Research and Innovation Programme under Grant GSA/GRANT/01/2016 (''FANTASTIC'').

ABSTRACT Precision Agriculture (PA) refers to applications asking for reliable and highly available precise positions, at centimeter level, in most of operational scenarios. Machinery guidance, automatic steering and controlled traffic farming enable machinery to move along repeatable tracks on the field, minimizing pass-to-pass errors and overlaps. In the recent years, satellite-based navigation has also opened the door to (semi) autonomous machineries for some specific farming scenarios and operations. Farming industry is now looking to use small robots to bring efficiencies and benefits to farms, capable of complex tasks that have not been possible with traditional large-scale agricultural machinery. Even though the state-of-the-art Real Time Kinematic (RTK) Global Navigation Satellite System (GNSS) receivers usually match the requirements posed by PA applications in open fields, propagation effects degrade the performance under foliage or with surrounding obstacles. This paper presents an experimental testbed and methodology suitable to assess the real performance of RTK GNSS-based devices in operational environments. Such testbed and methodology were effective to compare different devices, which resulted to be equivalent in open-sky conditions, but with significant differences in other types of environments. The paper also discusses opportunities and current limits of GNSS for emerging PA applications based on small robots and artificial intelligence.

INDEX TERMS Global navigation satellite system (GNSS), real time kinematic (RTK), horizontal position accuracy, positions availability.

I. INTRODUCTION

The accurate and reliable estimate of vehicles' position is at the basis of many applications for land transportation. In the last decade, it also became an important requirement in other domains, such as in Precision Agriculture (PA) that can be defined as the application of the ''*right treatment in the right place at the right time*'' [1] and allows for site-specific management and production optimization. Thanks to emerging digital technologies (e.g.: [2]–[5]), the modern agriculture is evolving and is becoming more and more efficient. Saving operational costs and reducing the environmental impact are the principal aspects of this evolution, which in turn results into more and better food production, while optimizing the whole agriculture processes.

PA is a growing market, whose automatic steering is the fastest growing segment as reported in [6]. Furthermore, the application of agricultural machinery in PA has experienced an increase in investment and research due to the use of robots for the execution of specific tasks [7]. Precision autonomous farming refers to the operation, guidance, and control of autonomous machines to carry out agricultural tasks. The reliable knowledge of such machines' position plays a crucial role for four main operations [7], namely guidance (i.e.: the way the machine navigates), detection (i.e.: the extraction of features from the environment), action (i.e.: the execution of the task) and mapping (i.e.: the construction of field maps with the most relevant features).

The associate editor coordinating the review of this manuscript and approving it for publication was Shuai Han.

Indeed, if the automatic machine has poor positioning capabilities, then it is not able to perform any path-following, path-tracking or trajectory-tracking activities. Without a precise knowledge of the actual position, autonomous navigation becomes dangerous for the vehicle integrity and, more importantly, for workers. Clearly, the design of autonomous machines demands for centimeter-level position accuracy in most of operational conditions. In turn, developers keep seeking innovative strategies and reliable systems at affordable costs to facilitate the penetration of PA solutions at large-scale. The Global Positioning System (GPS) - in general terms, the Global Navigation Satellite System (GNSS) - remains the main means for absolute positioning and outdoor navigation, but specific site conditions often pose challenges to the receivers. In fact, the presence of dense foliage and obstacles might induce signal attenuations and reflections that, in turn, cause corrupted measurements and degraded positioning performance. Even worse, in severe cases, the obstacles could reduce the number of visible satellites such that the GNSS receivers might be unable to provide Position Velocity and Time (PVT) data. In response to this issue, major manufacturers of GNSS antennas and receivers address the design of new components and signal processing algorithms able to mitigate the negative effects induced by the environment. Consequently, nowadays professional GNSS receivers are based on the processing of signals from multiple constellations (i.e.: GPS, Galileo, BeiDou and GLONASS), use correction services and often fuse GNSS measurements with other technologies. Today is already a common practice the integration of GNSS receivers with terrestrial sensors, namely wheel odometers [8], Inertial Navigation Systems (INSs) [9]–[13], cameras [14], and Light Detection and Ranging (LIDAR) [15]. Nonetheless, the performance assessment of innovative positioning technologies, algorithms and solutions in real scenarios characterized by dense foliage remains important to develop new automatic machines for PA applications.

The use of GNSS in agriculture has significantly expanded due to the increased availability of differential corrections. In order to assess suitability for precision agriculture, in [16] authors compared three modes of differential corrections through specific tests carried out in static and dynamic conditions. Such analysis confirmed that Real Time Kinematics (RTK) clearly provides the best performance and is the obvious choice if there are not constraints on the cost of the devices. When available, RTK base stations provide the highest level of position accuracy (cm range) and precision for agricultural tasks like mechanical intra-row weed control or thinning of crop plants, according to [17]. In [18], authors compared low-cost RTK receivers in order to investigate their application to precise agriculture. Moreover, in [19] researchers improved the previous work by evaluating the performance of RTK receivers set to use single or multi-GNSS constellation in typical agricultural sites, such as open fields, orchards and mountainous area. The use of Network RTK has also been investigated for precision farming, like in [20] for hilly areas.

This paper describes a possible approach to design an experimental testbed for the on-field validation of RTK GNSS-based devices employed as positioning modules in automatic machines. Such a testbed allows for reliable measurements and fair comparison of performance with respect to benchmarks. In addition to the testbed design, the paper will show that also the calibration and the testing procedures need to be carefully defined because of the centimeter-level positioning performance targeted by the devices under test. Indeed, small misalignments in the testbed installation, as well as poor accuracy of the calibration phase (e.g.: sub-centimeter errors in the estimate of the antennas' phase center), could lead to biased measurements and invalid test results. In this paper, we define a procedure to remove residual errors detected during the calibration phase. This method represents one of the main contributions of the paper since, according to author's knowledge, there are no previous works available in the scientific literature addressing such issue in practical experiments.

The paper is organized as follows: section II introduces relevant scenarios in the PA context, where the use of standalone GNSS is still problematic due to the lack of performance. These scenarios have been selected because they represent a challenge for the next generation of GNSS equipment and are suitable environments to host validation tests. Section III describes the proposed test methodology, details the functional block scheme of the experimental testbed, and introduces meaningful Key Performance Indicators (KPIs). Section IV presents a practical case where the proposed testing approach was employed to evaluate the performance of a high-end GNSS receiver prototype designed for professional applications. Section V presents and discusses the results of the tests, whereas Section VI concludes the paper highlighting the relevance of the presented work.

II. TEST SCENARIOS

This section presents and motivates the agricultural environments selected for the performance assessment and benchmarking of the RTK GNSS devices. The selection was driven mainly by the following aspects:

- *Signal propagation impairments posing technological challenges*: scenarios providing harsh conditions in terms of GNSS signal reception (e.g. presence of anti-hail nets and greenhouse covers, multipath, shadowing due to dense foliage) represented the desired test environment to challenge the devices under test;
- *Morphological conditions of the terrain*: in many applications, not only accurate positions matter, but also the estimated heading, namely the yaw, pitch and roll angles. Therefore, sloping and variable terrains provide perfect conditions where the RTK GNSS devices can be tested;

- *Productivity and territorial fallout*: scenarios representing local agricultural regions characterized by a relevant productivity are preferred. In addition, some sectors, like the wine sector, welcome innovations and new technologies more than others do.

These criteria have been applied in the selection of three distinct meaningful scenarios: open fields, presence of foliage (i.e.: vineyard, orchard) and greenhouse.

A. OPEN FIELDS

Systems for PA applications in open fields already benefit of a variety of high-end GNSS receivers and antennas. Indeed, there are many commercial devices, at different costs, able to match the main requirements of agriculture applications [6]. Limits of the horizontal position accuracy are in the 10÷30 cm range, like for spraying/spreading and harvesting in arable crops, down to 2.5 cm for automatic steering, control for precision operations such as planting [21], weeding, and in-row fertilization. Commercial high-end RTK GNSS receivers, able to process multi-constellation and multi-frequency signals already provide such performance. Thus, in this paper open sky conditions are often taken as reference for other more challenging scenarios.

B. PRESENCE OF FOLIAGE, E.G. VINEYARD AND ORCHARD

A GNSS-based device installed on an automatic machine moving along vineyard rows can be constrained by the poor visibility of satellites. In addition, it receives degraded GNSS signals due to leaves and obstacles surrounding the antenna. The same problems occur in orchards, which are generally characterized by higher tree heights (which further limit the visibility of satellites) and to the presence of anti-hail nets, like in Fig. 1. The relevance of this scenario is also due to the morphological characteristics of the terrain, since in some regions vineyards and orchards are in very steep hills, like in Fig. 2.

FIGURE 1. Orchard rows with anti-hail nets.

C. GREENHOUSE

Currently, the small robots used in greenhouses for specific tasks are not guided by satellite signals, rather they use ad-hoc technologies for indoor navigation, such as Ultra-Wide Band (UWB) modules. The coverage and the presence of obstacles cause attenuations and multipath, but these effects can be mitigated by new GNSS receiver technologies, which leverage on multi-GNSS, multi-frequency processing and enhanced algorithms.

FIGURE 2. Vineyard rows in steep terrain.

FIGURE 3. Typical greenhouse environment.

III. EXPERIMENTAL TESTBED AND METHODOLOGY

In order to assess the performance of new GNSS equipment in operational environments, we designed an experimental testbed that can host the devices under test, other devices taken as benchmark and measurement reference systems. This section presents the functional block diagram of such testbed and describes the main operations required to get reliable measurements.

A. FUNCTIONAL BLOCK DIAGRAM

Fig. 4 shows the functional block diagram of the experimental testbed.

The testbed includes:

- the GNSS receivers under test, each one connected to a GNSS antenna (or connected to more in case they feature multi-input antennas). Alternatively, the GNSS receivers can share a common GNSS antenna: the signal is split by a power splitter and sent to all receivers. When possible, this approach is preferable, as it guarantees equal signal conditions for all the receivers under test and fair comparison of the results. In addition to the PVT information, some GNSS receivers are able to estimate

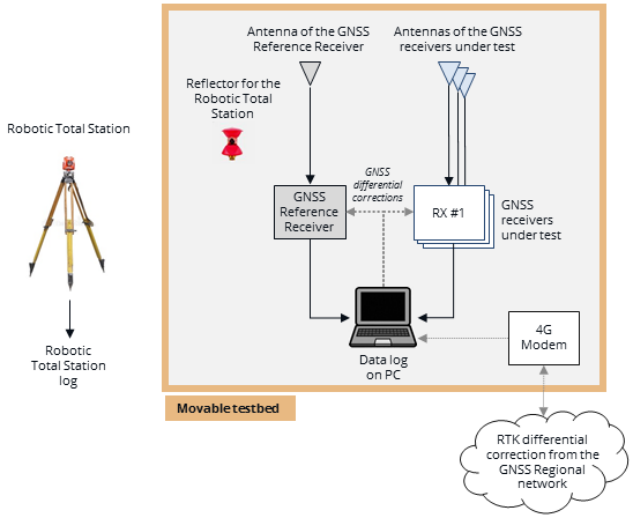

FIGURE 4. Conceptual block diagram of the experimental testbed designed for the on-field measurements and for the benchmarking of GNSS devices.

the attitude, i.e. the orientation with respect to the local level frame (horizontal plane) and true north: the testbed can evaluate also the attitude estimation error, if available from the receivers under test;

- a 4G modem that enables the connection to the internet, or to a base station, to retrieve local area differential GNSS corrections. All the tested receivers use the same DGNSS corrections, from a regional network of geodetic receivers (e.g. http://www.spingnss.it);
- two measurement reference systems (i.e.: one based on a robotic total station, one on GNSS technologies), which provide the estimate of positions, attitude and time with negligible errors, thanks to their superior performance with respect to the devices under tests. They are used to quantify the positioning and attitude estimation errors of the GNSS devices under test. It must be noticed that the attitude estimation from the GNSS measurement reference system is needed to proceed with the analysis of the positioning error, as detailed in Section III.D;
- a PC used to manage the internet connection, collect and distribute local area differential corrections to the receivers under tests. Such a PC can be used to log data either from the receivers under test and the GNSS-based reference system.

With the exclusion of the robotic total station, all components are mounted on a vehicle (labeled ''Movable testbed'' in Fig. 4), which moves on-field following a predefined trajectory.

It must be added that GNSS receivers can provide attitude estimations from the integration of external sensors (e.g. Inertial Measurement Units, IMU) or other strategies (e.g. multiple antennas). The presented testbed works independently from the strategy adopted by the receiver, so, in the following sections, the tested receivers will be referred to as GNSS receivers, independently from the presence of non-GNSS sensors.

B. SELECTION OF THE MEASUREMENT REFERENCE SYSTEMS

The choice of the measurement reference system is a key element in the design of the testbed due to the cm-level accuracy required by PA applications. Without a careful design of the testbed, the GNSS-based reference receiver could be affected by the same signal degradation of the GNSS receivers under test and would not be able to provide the reliable trajectory necessary to quantify the errors. On the other hand, alternative systems could have an insufficient performance level, or their use could be limited by the environmental characteristics. In order to cope with the scenarios listed and described in Section II, two complementary reference systems have been identified:

- a robotic total station tracking a reflector mounted on the testbed;
- a multi-frequency, survey-grade GNSS receiver combined with a tactical-grade Inertial Measurement Unit (IMU).

The robotic total station is able to provide an accurate position estimation independently from the availability of GNSS signals. A georeferenced and calibrated robotic total station sends a laser beam to a reflector mounted on a specific position of the testbed, then the robotic total station measures the laser round trip time, along with its direction of arrival. By processing these measurements, the precise position of the reflector is estimated. It is evident that such a system reaches optimal performance as long as no obstacles interfere with the correct transmission and reception of the laser beam: frequent and large obstacles might prevent the total station from tracking the reflector correctly. This makes the robotic total station suitable in the greenhouse and flat orchard rows, where GNSS signals are obscured by the greenhouse cover or leaves of high plants. On the contrary in steep vineyards, the GNSS-based reference system is preferred, if this can work in conditions of open sky. Indeed, to avoid the signal degradation due to the leaves of the grapevine, the antenna of the GNSS-based reference was mounted on a pole higher than the vineyard rows, which grants a good visibility of the satellites.

C. KEY PERFORMANCE INDICATORS

The experimental testbed introduced in the previous section is suitable for the collection of data sets, which can be processed off-line to quantify the positioning performance of the devices, according to predefined Key Performance Indicators (KPI). The first KPI is the Horizontal Position Error (HPE) and is defined as a complex number, with the error on the East coordinate on the real axis, and the error on the North coordinate on the imaginary axis:

$$\varepsilon = (x_i^E - x_{ref}^E) + j(y_i^N - y_{ref}^N) \quad (1)$$

where:

- x_i^E is the East coordinate estimated by the i-th receiver under test and referenced to the antenna's phase center of the GNSS-based reference receiver, or to the reflector of the robotic total station;
- x_{ref}^E is the East coordinate estimated by the measurement reference system;
- y_i^N is the North coordinate estimated by the receiver under test and referenced to the antenna's phase center of the GNSS-based reference receiver, or to the reflector of the robotic total station;
- y_{ref}^N is the North coordinate estimated by the measurement reference system.

Considering a data collection spanning over a specific time interval, we evaluated the cumulative distribution (Cumulative Distribution Function, CDF) of the HPE magnitude (expressed in meters), along with its mean value, standard deviation (std) and the 50$^{\text{th}}$ and 95$^{\text{th}}$ percentiles.

The second KPI we evaluated is the availability of the PVT data. To evaluate this KPI, only the estimates able to match the accuracy requirements of the scenario under evaluation are taken into account. Therefore, the availability is defined as:

$$\mathrm{A}_i = \frac{\mathrm{n}_i}{\mathrm{R}_i \mathrm{T}} \cdot 100 \tag{2}$$

where n_i represents the number of PVT data epochs within the accuracy limit in a pre-defined time window T and R_i is the PVT output rate of i-th GNSS receivers under test. A_i is dimensionless and expressed as a percentage.

Specific KPIs for the assessment of the ambiguity resolution performance have not been considered, because the quality of the ambiguity resolution directly affects both the HPE and the availability.

One of the receivers under test was capable to estimate the attitude of the vehicle by interferometric and inertial techniques. The error on this attitude estimation could also be evaluated. For the roll, pitch and yaw, we compute such error as the difference between the angles estimated by the measurement reference system and those estimated by the receiver under test:

$$\varepsilon_{a,\mathrm{i}} = a_i - a_{ref} \tag{3}$$

where:

- a_i is the angle estimated by the i-th GNSS receiver under test. It can represent the roll, the pitch or the yaw;
- a_{ref} is the corresponding angle estimated by the measurement reference system.

Also for the attitude angles, assuming a data collection spanning over a specific time interval, we used the mean value and the 95$^{\text{th}}$ percentile as metrics to quantify and compare performance. Differently from the position estimation, the attitude is not an output always available from all GNSS receivers, so this KPI should be considered only when the tested receivers evaluate the attitude. In the remaining part of the paper, ε_y, ε_p, and ε_r will indicate the yaw, pitch and roll errors.

D. PROJECTION OF THE ESTIMATED COORDINATES TO THE REFERENCE SYSTEM TRAJECTORY

The computation of the HPE requires that the estimated coordinates of the receiver under test are projected either to the antenna's phase center of the GNSS reference receiver or to the position of the reflector of the robotic total station. This is possible because the level arms between the antennas' phase centers (and reflector) can be measured once the devices are installed on the vehicle and the attitude is known from the measurement reference system. The lever arm $\boldsymbol{l}_i^b$ is defined as the vector that runs from the phase center of the antenna of the i-th GNSS receiver under test to the phase center of the reference antenna (or the reflector). $\boldsymbol{l}_i^b$ is expressed in the body frame (note the apex b) and is assumed to be constant over time. After the installation of the devices and the measure of the lever arms, the position of the i-th receiver's antenna, computed in the navigation frame (note the apex n), is translated to the GNSS antenna of the reference receiver (or reflector) through the following expression:

$$\hat{\boldsymbol{p}}_i^n = \boldsymbol{p}_i^n + \boldsymbol{R}_b^n \boldsymbol{l}_i^b \tag{4}$$

where:

- $\hat{\boldsymbol{p}}_i^n$ represents the vector of coordinates (in the navigation frame) of the i-th receiver under test, projected to the phase center of the GNSS antenna of the reference receiver (or the reflector);
- $\boldsymbol{p}_i^n$ represents the vector of coordinates in the navigation frame estimated by the i-th GNSS receiver under test;
- $\boldsymbol{R}_b^n$ is the direction cosine matrix representing the rotation between the body and the navigation frames, as available from the inertial reference system. $\boldsymbol{R}_b^n$ is obtained from the attitude evaluated by the GNSS measurement reference system;
- $\boldsymbol{l}_i^b$ is the lever arm vector associated to the phase center of the antenna of the i-th GNSS receiver under test and expressed in the body frame.

Then, the new estimated position vector $\hat{\boldsymbol{p}}_i^n$ is converted to Universal Transverse Mercator (UTM) *easting*, *northing* and *up* coordinates $\hat{\boldsymbol{p}}_i^u = \left(\hat{x}_i^E, \hat{y}_i^N, \hat{z}_i^U\right)$ and can be compared with the position estimated by the reference system in the same coordinate frame $\boldsymbol{p}_{ref}^u = \left(x_{ref}^E, y_{ref}^N, z_{ref}^U\right)$, according to (1).

E. EXPERIMENTAL SYSTEM CALIBRATION

The projection of coordinates described in III-E is based on the measure of the lever arm, which can be corrupted by errors. Indeed, the measured lever arm can be rewritten as:

$$\boldsymbol{l}_i^b = \boldsymbol{l}_{i,true}^b + \boldsymbol{\varepsilon}_{l,i} \tag{5}$$

where $\boldsymbol{\varepsilon_{l,i}}$ represents an unknown error (bias), which also includes possible variations of the antennas' phase centers. A poor estimation of the lever arm generates an erroneous computation of the HPE. Therefore, it is necessary to compensate any bias on the measured phase centers' lever arm, which should be known with mm-level accuracy, before assessing the performance of the GNSS receiver under test.

The effects of this lever arm error are emphasized when the testbed moves along an 8-figure trajectory, like that depicted in Fig. 5. In such a case, the error $\boldsymbol{\varepsilon}_{l,i}$ corrupts either the easting and northing components of the HPE and is strongly correlated to the period of such 8-figure. Fig. 6 shows the easting and northing components of the HPE for four different GNSS receivers under test, plotted with different colors. In this case all the receivers share the same antenna, therefore the same lever arm error affects the receivers position estimates (and the index i is omitted in the following of this section).

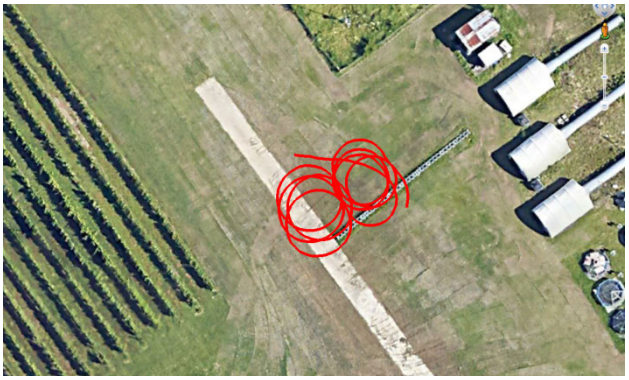

FIGURE 5. Sample of an 8-figure trajectory as those used by the calibration procedure.

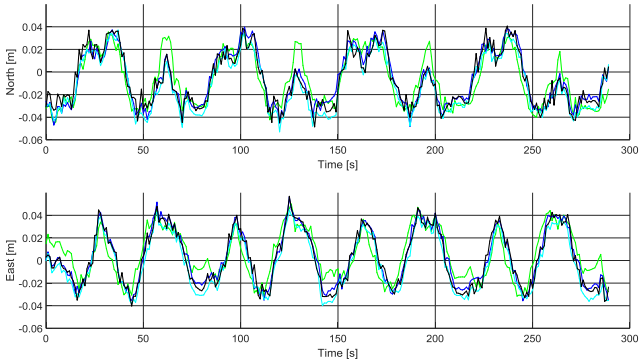

FIGURE 6. HPE along easting and northing coordinates for four GNSS receivers under test (plotted with different colors), with a residual error $\boldsymbol{\varepsilon}_l$ in the phase centers' lever arm.

Clearly, a cm-level recursive error pattern is visible in both the easting and northing coordinates. Such a pattern is the same for all the GNSS receivers and has a period which corresponds to the period of the 8-figure trajectory, along which the testbed moved.

The detection of such recursive pattern in the HPE components is invaluable to estimate $\boldsymbol{\varepsilon}_l$ and in turn $\boldsymbol{l}^b_{true}$. Indeed, the best estimate of the phase centers' lever arm can be found in post processing by searching for the value that minimizes the error on the HPE easting and northing components. Fig. 7 shows the mean of the absolute value of the HPE, for different values of the lever arms, which is varied along the x-axis and y-axis in the body frame. In other words, each

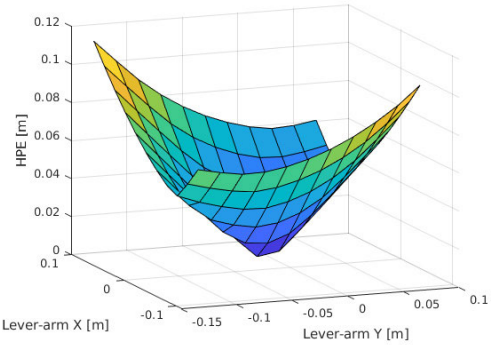

FIGURE 7. Absolute value of the HPE varying the lever arm along the x- and y- axes in the body frame.

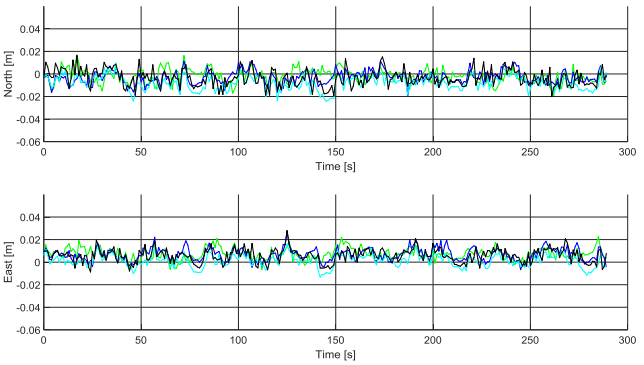

FIGURE 8. HPE along easting and northing coordinates for four GNSS receivers under test (plotted with different colors), after the correction of $\boldsymbol{\varepsilon}_l$.

cell of the XY-plane corresponds to a different $\boldsymbol{l}^b$, which is used to compute the HPE. The mean of the absolute value is plotted and the cell corresponding to the minimum is taken, as it indicates the best estimate of the lever arm that minimizes the error $\boldsymbol{\varepsilon}_l$.

Fig. 8 is the same plot of Fig. 6, but using the refined estimate of the lever arm. The recursive pattern is no longer visible, and the easting and northing components of the HPE are noisy and bounded within the sensitivity of the reference system. After the described process, an estimation of $\boldsymbol{l}^b_{true}$ is available and is used for the assessment of the receiver performance.

IV. PRACTICAL EXPERIENCE IN REAL AGRICULTURAL CONTEXTS

The experimental testbed and methodology described in Section III were used in the frame of the FANTASTIC project [22] to evaluate the performance of a new prototype, which is a triple-frequency, multiple-constellations, GNSS receiver targeted to PA applications. Such a GNSS receiver can be connected to two wideband antennas, with exceptionally stable phase center. One of them is equipped with a tactical grade Micro Electro-Mechanical Systems (MEMS) IMU. The collocation of the IMU in the antenna has several advantages: among all, it avoids the need for a precise estimation

of the antenna to IMU lever arm, easing the installation procedure. The GNSS receiver runs a state-of-the-art GNSS/INS loosely coupled integration, which uses high accuracy RTK position estimates, as well as GNSS attitude estimates to aid the INS heading estimation during motion. The developed system does not require an initialization procedure of the attitude, which would typically involve vehicle motion with sufficient velocity to deduce the heading from the course over ground. Especially in PA applications, such an initialization procedure is impractical.

Following the general block diagram of Fig. 4, the implemented testbed included:

- the new prototypal GNSS receiver, connected to its own two antennas. It will be indicated as *FANTASTIC receiver* or, in short, *FANTASTIC*;
- three state-of-the art high-end commercial receivers that could be considered benchmark devices. All of them are able to process concurrent signals from different GNSS constellations (i.e.: GPS and Galileo), over at least two frequencies (i.e. L1/E1, L2) and provide RTK measurements. They are connected to the same antenna, through a passive RF splitter, to have equal signal conditions. In the remaining part of the paper these benchmark receivers will be indicated as *Bmk 1*, *Bmk 2*, and *Bmk 3*. Further details about benchmark receivers are not given to avoid disclosing sensitive commercial info;
- as GNSS-based reference system, we selected a GNSS+INS high-end receiver able to provide Root Mean Square (RMS) error less than 2 cm. It is generally employed in professional applications, in experimental systems [12] and is often used for scientific investigations. It will be indicated as *GNSS Reference Receiver*;
- a survey grade robotic total station able to provide distance and angle estimations with a standard deviation of the error near to 1 mm and 10^{-3} deg respectively, in optimal environmental conditions. It will be indicated as *Robotic Total Station*.

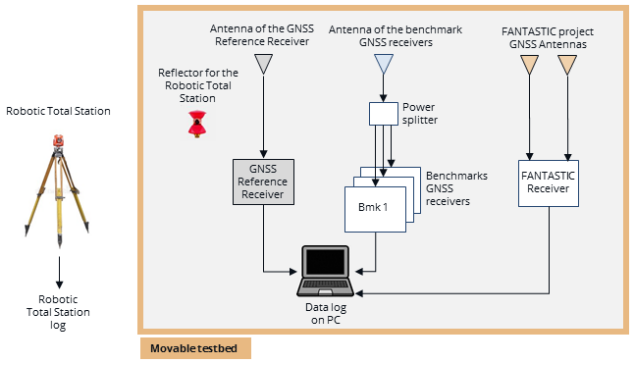

FIGURE 9. Block diagram of the experimental set up implemented in the frame of the FANTASTIC project.

Fig. 9 follows Fig. 4 and shows the functional scheme of the implemented testbed, where the blocks related to the distribution of the RTK corrections are omitted for sake of simplicity. The testbed, with the exclusion of the Robotic Total Station, is mounted on a remoted controlled electric vehicle, designed for agricultural works.

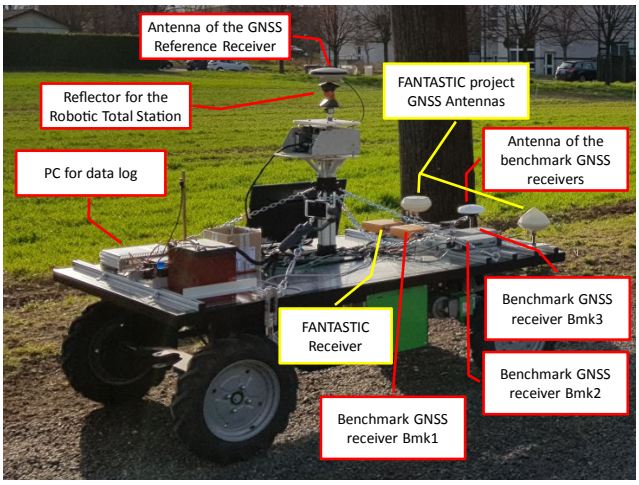

FIGURE 10. Experimental system used for the on-field test in a greenhouse.

Fig. 10 shows the experimental system installed on the electrical vehicle. It is possible to see three antennas at the front edge of the vehicle, where the central one is connected to the benchmark receivers through a passive splitter. All the GNSS receivers are installed just behind these antennas, whereas the central pole hosts the GNSS Reference Receiver and its antenna. Note that the prism enabling the tracking of the Robotic Total Station is visible right below such antenna. Finally, the car PC for data logs and batteries are placed on the back of the vehicle.

V. RESULTS AND DISCUSSION

This section reports a set of the main results. For the sake of clarity, they are divided into subsections, according to the scenarios introduced in Section II.

A. OPEN FIELDS

The open sky conditions experienced following the trajectory in Fig. 11 are representative of open fields: at the location and time of this test, up to 13 satellites were visible with a best Position Dilution Of Precision (PDOP) equal to 1.6 (see Fig. 26 in the Appendix for details). In such conditions, we used the GNSS Reference Receiver.

Fig. 12 shows the cumulative distribution of the HPE magnitude for the FANTASTIC Receiver (green curve) and the three benchmarks. As expected in open sky conditions, the receivers show comparable performance, with the 50^{th} and 95^{th} percentiles approximately equal to 1.5 cm and 3 cm, respectively.

Considering a position accuracy limit of 2.5 cm, we observed the FANTASTIC receiver provided data within such limit for 92.5% of time, similarly to Bmk 1. The other two receivers used as benchmarks had a lower availability, approximately equal to 85.5%.

FIGURE 11. Trajectory followed during the data collection in open sky conditions.

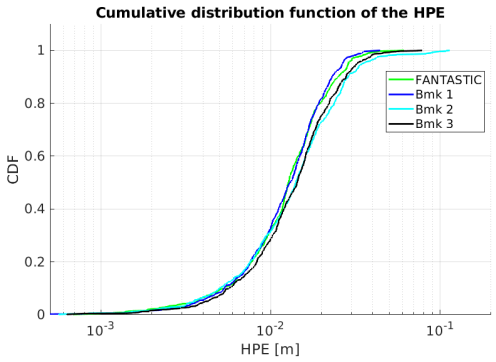

FIGURE 12. CDF of the HPE for the receivers under test in open sky conditions.

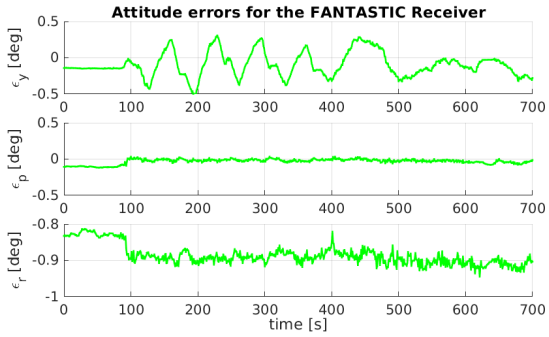

FIGURE 13. Attitude errors of the FANTASTIC receiver in open sky condition.

Fig. 13 reports the heading errors of the FANTASTIC receiver with respect to the GNSS Reference Receiver, according to the KPI defined in III-D. As shown, the yaw and pitch errors are always bounded to 0.5 deg, whereas the error on the roll shows a bias approximately equal to -0.9 deg. After further investigations, such bias was due to a misalignment between the electric vehicle hosting the testbed and the case of the reference system antenna. Fig. 13 confirms good performance of the FANTASTIC receiver. Indeed, they are comparable to those of the GNSS Reference Receiver, which is more expensive and belongs to a superior class of equipment.

B. ENVIRONMENT CHARACTERIZED BY THE PRESENCE OF FOLIAGE

Tests have been performed in two different environments where the GNSS signal is obstructed by the presence of foliage: a kiwifruit orchard and a vineyard. In both cases the positioning and attitude errors were estimated by using the GNSS Reference Receiver, which was mounted on a pole to have a better visibility of the sky, as visible in Fig. 14.

FIGURE 14. Testbed used in vineyard, with GNSS-based reference system mounted on a pole to gain good visibility of the sky.

The kiwifruit orchard that hosted the tests is located in Lagnasco, Italy; Fig. 15 shows the map along with the trajectory followed by the testbed. At the location and time of this test, up to 12 satellites were visible with a best PDOP equal to 1.4 (see Fig. 27 in the Appendix for details)

FIGURE 15. Trajectory followed during the test in a kiwifruit orchard.

Fig. 16 and Fig. 17 show the cumulative distribution function of the HPE and the time plot of the attitude errors respectively.

The comparison with Fig. 12 and Fig. 13 allows to conclude that the positioning errors are higher than in the open sky conditions, but their magnitude is however within 10 cm most of the time, whereas the attitude errors are comparable. This could be explained by considering that this orchard

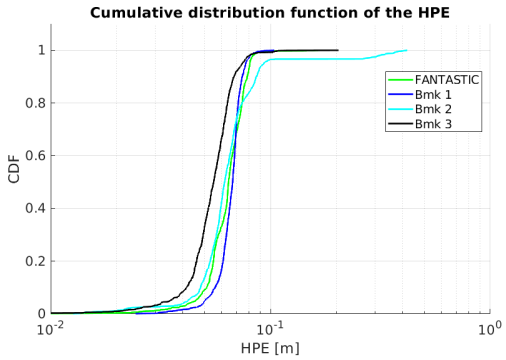

FIGURE 16. CDF of the HPE for the receivers under test in a kiwifruit orchard.

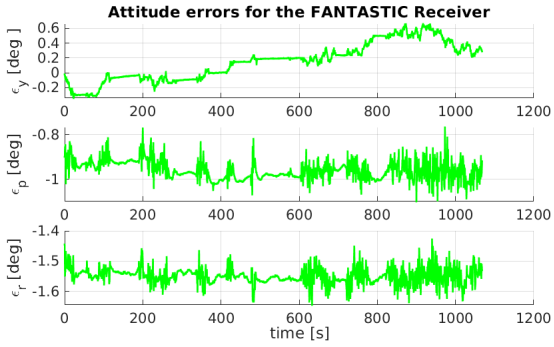

FIGURE 17. Attitude errors of the FANTASTIC receiver in a kiwifruit orchard.

FIGURE 18. Three-dimensional representation of the trajectory followed during the test in vineyard.

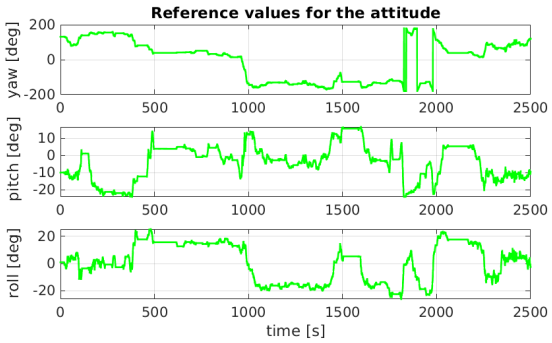

FIGURE 19. Attitude values in the vineyard.

is characterized by the presence of a dense foliage, with a moderate height of the trees. Consequently, the GNSS signal is shadowed, but not blocked or degraded to induce receivers to lose the signal tracking. This is confirmed by the KPI metrics reported in Table 1 in the Appendix. The horizontal positioning error is under the 10 cm for almost 100% of the time, as highlighted by the availability (i.e.: 96.4% is the worst availability measured for Bmk 2) and the percentiles (i.e.: 9.3 cm is the worst 95th percentile measured for Bmk 2).

The mean of the attitude errors stays below 1 degree for the yaw and pitch, and is approximately equal to 1.5 degree for the roll. Also in this case, we noted a slight degradation of performance w.r.t. the open fields case and we still observed the presence of the small misalignment affecting the roll estimation, as reported in Section V.A.

The vineyard where we performed the test is located in Serralunga d'Alba, Italy, whose picture is reported in Fig. 18: at the location and time of this test, up to 16 satellites were visible with a best PDOP equal to 1.2 (see VI in the Appendix for details). Such environment featured a couple of peculiar characteristics, making it different from the previous case:

- the vineyard is in an extremely steep side of a hill (i.e.: the maximum pitch is 24 deg), therefore the pitch and roll angles assume values higher than in the case of the kiwifruit orchard (Fig. 19).
- the rural environment posed limitations to the cell phone network coverage, making difficult the possibility to retrieve differential corrections from internet services or from a base station.

The limited availability of differential corrections prevented the RTK positioning, which resulted in degraded positioning performance w.r.t. the previous case. Nevertheless, for two receivers of the testbed (i.e.: FANTASTIC and Bmk 1) we were able to store raw measurements (i.e.: pseudoranges, carrier phase measurements, etc.), apply differential corrections off-line and then evaluate the RTK positioning performance. Taking this into account, we present either the performance obtained in Real Time (RT) and in Post Processing (PP). Also the GNSS Reference Receiver suffered from the lack of differential corrections. In order to get a reliable error analysis, also the raw measurements of the GNSS Reference Receiver were post processed and the resulting RTK positioning is used for the error analysis. For sake of clarity, it must be noticed that PP results were obtained by proprietary tools from the receiver manufacturers, whereas the RT results are those recorded by the receivers on the field. Such proprietary tools were not available for Bmk 2 and Bmk 3, whose PP performance were consequently not analyzed.

Fig. 20 reports the cumulative distribution function for both the RT (a) and PP (b). In the RT case, the degradation of performance is evident, and also the gap between different receivers widens. Indeed, FANTASTIC and Bmk 3 show

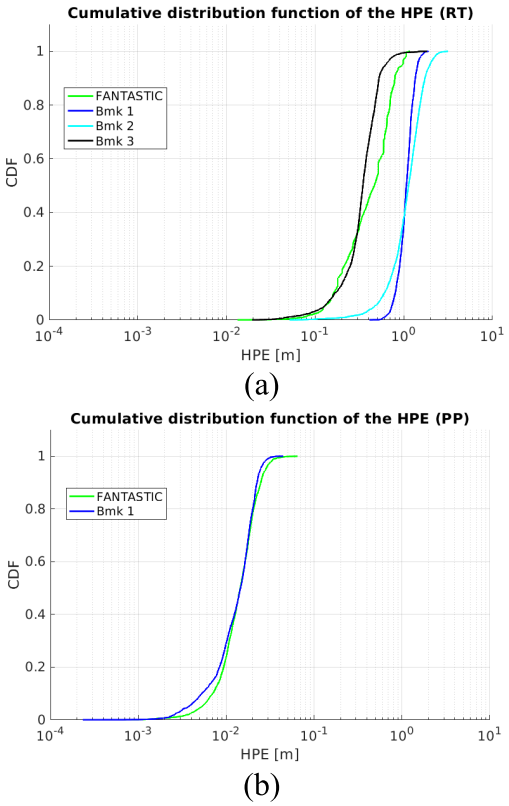

FIGURE 20. CDF of the HPE for the receivers in the vineyard, real time results (a) and post processing results (b).

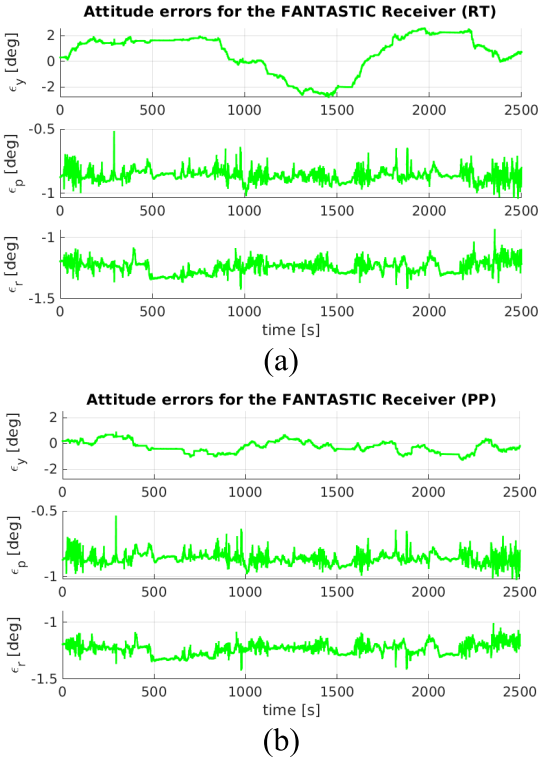

FIGURE 21. Attitude errors of the FANTASTIC Receiver in the vineyard, real time results (a) and post processing results (b).

similar errors which are smaller than those reached by Bmk 1 and Bmk 2. For example, the mean HPE goes from 36 cm for Bmk 3 to 116 cm for Bmk 2. As expected, the analysis carried out off-line exhibits great improvements for what concerns the position accuracy of FANTASTIC and Bmk 1 receivers, which reaches levels comparable to the open sky conditions (Fig. 12). The mean HPE for the FANTASTIC receiver is equal to 1.5 cm (96% reduction w.r.t. RT) and reaches 1.4 cm for the Bmk 1 (98% reduction w.r.t. RT). Similar comments can be made observing the values of percentiles, as reported by the full statistics of Table 2 in the Appendix.

The attitude errors are reported in Fig. 21 for the RT estimation and the PP, respectively. Pitch and roll estimations do not improve when PP is adopted, whereas the mean error on the yaw estimate passes from 2.5 deg to 0.9 deg, with a 64% reduction.

Finally, the analysis of the availability metric leads to the conclusion that RTK is necessary to reach the performance level required by PA: without RTK, the availability, either with 2.5 cm and 10 cm thresholds for the maximum error, is zero or negligible. On the contrary, RTK allows to reach positioning errors under 2.5 cm for the 90.5% and 95.7% of the time in the case of FANTASTIC and Bmk 1 respectively.

C. GREENHOUSE

Fig. 22 shows the greenhouse where the experimental testbed was used to evaluate the performance of the FANTASTIC Receiver and the benchmark devices: the electric cart hosting the testbed entered the greenhouse and moved through it following a straight trajectory, back and forward. The greenhouse metal structure and coated glasses represented a challenging scenario for all the GNSS receivers under test, as the signals from the satellites were attenuated by 15-20 dB and reflected and, consequently, all the GNSS receivers under test experienced a complete outage for the most part of the test duration. Obviously, this was true also for the GNSS Reference Receiver. Indeed, Fig. 23 shows the positions estimated by the GNSS Reference Receiver: few seconds after the testbed entered the greenhouse, the position estimated by the GNSS Reference Receiver quickly drifted away. This result is not unexpected: as already pointed out in [12], even professional reference systems based on GNSS high-end receivers and tactical grade inertial sensors suffer during GNSS signals outages or degraded signals. In such conditions, additional sensors not based on satellite signals, can improve the reliability and precision (e.g., in [12] an odometer is considered). In such conditions, the most appropriated reference system was the Robotic Total Station. During the data collection, that lasted for about 270 seconds, such reference system recorded the track reported in Fig. 24, which is overlapped to an orthophoto of the greenhouse.

By considering the Robotic Total Station as the reference, it was possible to compute the positioning error for the receivers under test, whereas the error related to the attitude estimation could not be evaluated because the total station did not output the attitude of the electric vehicle.

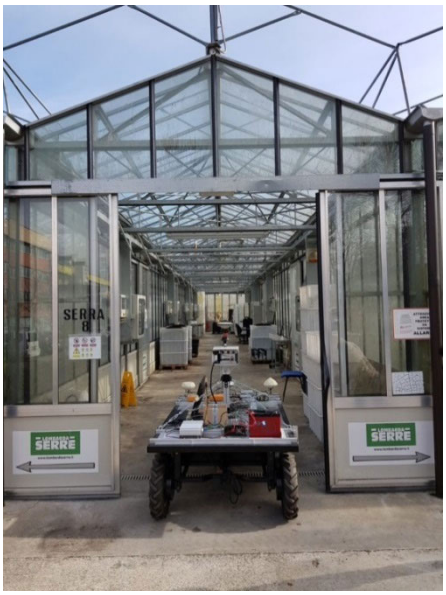

FIGURE 22. Electric vehicle hosting the experimental testbed entering the greenhouse main door.

FIGURE 23. Position estimated by the GNSS Reference Receiver overlapped to an orthophoto of the greenhouse.

Fig. 25 reports the cumulative distribution function of the HPE: the magnitude of the errors is the greatest amongst the test reported in this paper. This is confirmed by the statistics reported in Table 3 of the Appendix. Only the FANTASTIC Receiver was able to maintain a mean HPE within 1 m, whereas the best benchmark receiver, i.e. Bmk 2, was able to reach a mean HPE approximately equal to 1.3 m. Such trend is the same observing the percentiles: Bmk 1 and Bmk 3 have a 95th percentile beyond 5 m and 8 m respectively. Finally, the availability is very reduced: only the FANTASTIC Receiver is able to grant an availability over the 10 % but just for the 10 cm threshold, which remain poor for the target PA operations in greenhouse.

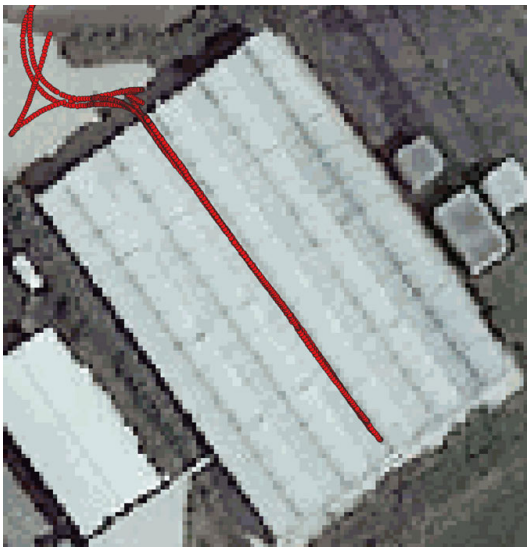

FIGURE 24. Reference positions estimated by the robotic total station overlapped to an orthophoto of the greenhouse.

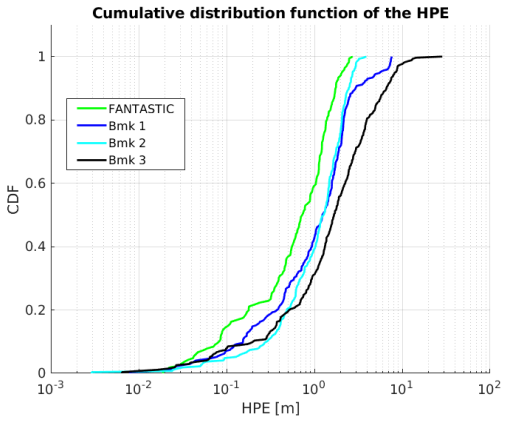

FIGURE 25. CDF of the HPE for the receivers under test in the greenhouse.

VI. CONCLUSION

This paper has presented an experimental testbed and methodology that enabled the on-field evaluation of performance of RTK GNSS-based devices devoted to PA applications. The key point was the choice and setting of a reference system able to provide reliable measurements of positions and attitude, which were used as reference in the errors computation. The selection of the reference system is performed off-line and depends on the type of environment (i.e.: open field, constrained environment with objects surrounding the antenna, indoor), in which the tests have to be performed. An accurate design of the testbed layout and a calibration procedure have been described, as they were fundamental to quantify small errors, on the order of few centimeters for positions and few degrees for attitude.

The experimental testbed and methodology were designed to assess performance of the devices under test directly in operational agriculture environments. Although problems

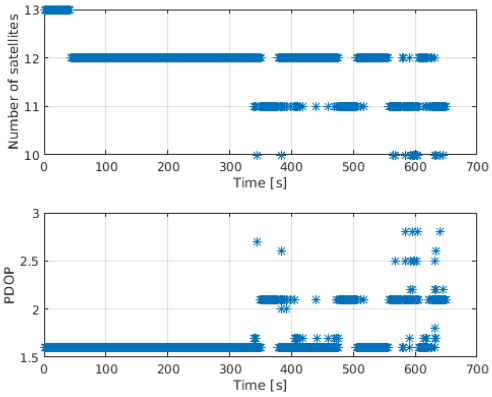

FIGURE 26. Number of satellites used in the PVT computation and PDOP for the open sky dataset.

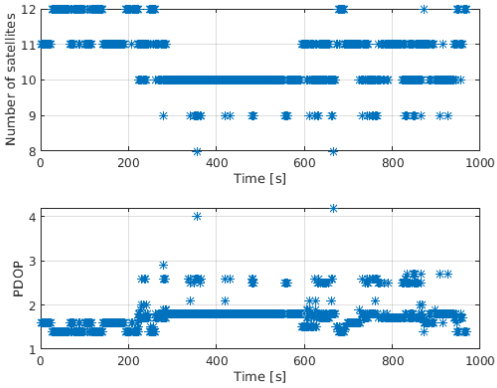

FIGURE 27. Number of satellites used in the PVT computation and PDOP for the dataset in the kiwifruit orchard.

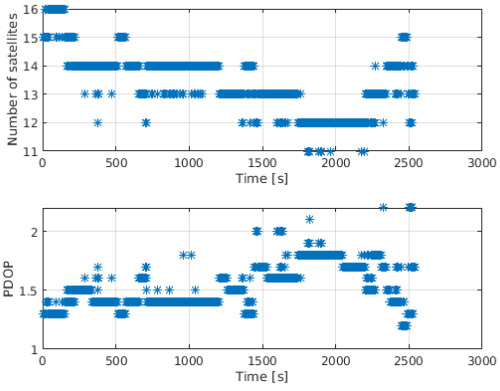

FIGURE 28. Number of satellites used in the PVT computation and PDOP for the dataset in the vineyard.

related to the setting of a reliable reference system could be overcome by using an in-lab test setup (where the GNSS signals are generated by using a hardware signal generator), this approach could have some limits when the set up include inertial sensors or special environments and dynamics (e.g.: greenhouse, steep terrain) that need to be reproduced. Furthermore, as highlighted by the results presented in this paper, the devices under test were based on the fusion of multiple sensors and revealed their major benefits in the presence

TABLE 1. KPI metrics for the tested receivers under the foliage of a kiwifruit orchard.

	Device under test			
KPI metric	FANTASTIC	Bmk 1	Bmk 2	Bmk 3
Availability at 2.5 cm	0.7%	0.1%	2.4%	2.0%
Availability at 10.0 cm	99.7%	99.8%	96.4%	99.1%
HPE mean [cm]	6.4	6.6	7.2	5.5
HPE std [cm]	1.3	0.8	5.1	1.3
HPE 50^{th} perc. [cm]	6.4	6.7	6.2	5.5
HPE 95^{th} perc. [cm]	8.1	7.7	9.3	7.4
Yaw error mean [deg]	0.15	-	-	-
Yaw error 95^{th} perc. [deg]	0.56	-	-	-
Pitch error mean [deg]	-0.96	-	-	-
Pitch error 95^{th} perc. [deg]	1.02	-	-	-
Roll error mean [deg]	-1.55	-	-	-
Roll error 95^{th} perc. [deg]	1.59	-	-	-

of real harsh environments, or even during GNSS signal outages. In these cases, the in-lab evaluation of performance of RTK GNSS-based devices could be impractical or come at high costs.

The results reported in this paper have demonstrated that the proposed testing approach was successful to evaluate (and benchmark) the performance of a new GNSS receiver prototype devoted to the PA applications. As expected, its performance was comparable with benchmarks in open sky, but showed differences in other environments. The new prototype demonstrated superior performance w.r.t. state-of-the art, especially for what concerns attitude determination, with 95^{th} percentiles lower than 1 deg for the heading, lower than 0.4 deg for the pitch and lower than 0.2 deg for the roll, respectively. Under foliage, either in orchard and vineyard, the prototype guaranteed positioning errors lower than 2.5 cm for 90% of time, and lower than 10 cm for 99% of time.

Last, the test campaign, performed in real agriculture environments, highlighted some limits due to external factors, rather than the devices under test themselves. RTK GNSS-based devices can match target performance requirements and, in turn, be used for machinery guidance and automatic field operations, only with reliable wireless channels and mobile network coverage. From the performed test campaign, this seems not always the case, since in one of the presented tests all receivers struggled to receive differential corrections with consequent degraded performance, either for positioning

TABLE 2. KPI metrics for the tested receivers under foliage in vineyard. Where post processing is available, the statistics for both Real Time elaboration (RT) and Post Processing (PP) are reported.

	Device under test					
	FANTASTIC		Bmk 1		Bmk 2	Bmk 3
KPI metric	RT	PP	RT	PP		
Availability at 2.5 cm	0.1%	90.5%	0.0%	95.7%	0.0%	0.3%
Availability at 10.0 cm	2.4%	100%	0.0%	100%	0.1%	3.3%
HPE mean [cm]	47.1	1.5	107.6	1.4	116.4	36.2
HPE std [cm]	25.3	0.7	21.5	0.6	45.5	16.4
HPE 50^{th} perc. [cm]	46.6	1.4	106.8	1.5	113.0	34.5
HPE 95^{th} perc. [cm]	96.6	2.8	143.5	2.4	197.4	62.0
Yaw error mean [deg]	0.6	-0.3	-	-	-	-
Yaw error 95^{th} perc. [deg]	2.5	0.9	-	-	-	-
Pitch error mean [deg]	-0.9	-0.9	-	-	-	-
Pitch error 95^{th} perc. [deg]	0.9	0.9	-	-	-	-
Roll error mean [deg]	-1.2	-1.2	-	-	-	-
Roll error 95^{th} perc. [deg]	1.3	1.3	-	-	-	-

TABLE 3. KPI metrics for the tested receivers in the greenhouse.

	Device under test			
	FANTASTIC	Bmk 1	Bmk 2	Bmk 3
Availability at 2.5 cm	1.8%	1.5%	1.1%	1.5%
Availability at 10.0 cm	14.5%	7.0%	4.8%	7.5%
HPE mean [cm]	86.3	159.3	131.5	267.5
HPE std [cm]	65.2	162.6	82.6	306.6
HPE 50^{th} perc. [cm]	72.7	123.9	128.5	167.4
HPE 95^{th} perc. [cm]	207.3	555.5	272.0	812.7

(95^{th} percentile approximately equal to 1 m) and attitude (95^{th} percentile higher than 1 deg).

APPENDIX

See Figures 26–28 and Tables 1–3.

REFERENCES

[1] V. Adamchuk, "Precision agriculture and food security," in *Proc. Global Agenda Space Secur. Workshop Bringing Space Down Earth*, Montreal, QC, Canada, Jul. 2013.
[2] S. Ivanov, K. Bhargava, and W. Donnelly, "Precision farming: Sensor analytics," *IEEE Intell. Syst.*, vol. 30, no. 4, pp. 76–80, Jul. 2015.
[3] R. Dolci, "IoT solutions for precision farming and food manufacturing: Artificial intelligence applications in digital food," in *Proc. IEEE 41st Annu. Comput. Softw. Appl. Conf. (COMPSAC)*, Jul. 2017, pp. 384–385, doi: 10.1109/compsac.2017.157.
[4] M. Dholu and K. Ghodinde, "Internet of Things (IoT) for precision agriculture application," in *Proc. 2nd Int. Conf. Trends Electron. Informat. (ICOEI)*, May 2018, pp. 339–342, doi: 10.1109/icoei.2018.8553720.
[5] A. Khaliq, L. Comba, A. Biglia, D. Ricauda Aimonino, M. Chiaberge, and P. Gay, "Comparison of satellite and UAV-based multispectral imagery for vineyard variability assessment," *Remote Sens.*, vol. 11, no. 4, p. 436, Feb. 2019.
[6] *GNSS Market Report*, European GNSS Agency, Prague, Czech Republic, no. 5, 2017.
[7] F. A. Auat Cheein and R. Carelli, "Agricultural robotics: Unmanned robotic service units in agricultural tasks," *EEE Ind. Electron. Mag.*, vol. 7, no. 3, pp. 48–58, Sep. 2013, doi: 10.1109/mie.2013.2252957.
[8] D. M. Bevly and S. Cobb, *GNSS for Vehicle Control*. Boston, MA, USA: Artech House, 2009.
[9] D. H. Titterton and J. L. Weston, *Strapdown Inertial Navigation Technology*, 2nd ed. Reston, VA, USA: American Institute of Aeronautics and Astronautics, 2004.
[10] P. Aggarwal, Z. Syed, A. Noureldin, and N. El-Sheimy, *MEMS-Based Integrated Navigation*. Norwood, MA, USA: Artech House, 2010.
[11] M. Shafiq, "GNSS/INS integration in urban areas," Ph.D. dissertation, Norwegian Univ. Sci. Technol., Trondheim, Norway, Apr. 2014.
[12] G. Falco, M. Nicola, and M. Pini, "Positioning based on tightly coupled multiple sensors: A practical implementation and experimental assessment," *IEEE Access*, vol. 6, pp. 13101–13116, 2018.
[13] G. Falco, M. Pini, and G. Marucco, "Loose and tight GNSS/INS integrations: Comparison of performance assessed in real urban scenarios," *Sensors*, vol. 17, no. 2, p. 255, Jan. 2017.
[14] S. Zaman, L. Comba, A. Biglia, D. R. Aimonino, P. Barge, and P. Gay, "Cost-effective visual odometry system for vehicle motion control in agricultural environments," *Comput. Electron. Agricult.*, vol. 162, pp. 82–94, Jul. 2019.
[15] C. Qian, H. Liu, J. Tang, Y. Chen, H. Kaartinen, A. Kukko, L. Zhu, X. Liang, L. Chen, and J. Hyyppä, "An integrated GNSS/INS/LiDAR-SLAM positioning method for highly accurate forest stem mapping," *Remote Sens.*, vol. 9, no. 1, p. 3, Dec. 2016.
[16] P. I. Coyne, S. J. Casey, and G. A. Milliken, "Comparison of differentially corrected GPS sources for support of site-specific management in agriculture," Kansas State Univ., Manhattan, KS, USA, Kansas Agricult. Exp. Station SP 03-419, Jan. 2020. [Online]. Available: https://krex.k-state.edu/dspace/handle/2097/38240
[17] H. Sun, D. C. Slaughter, M. P. Ruiz, C. Gliever, S. K. Upadhyaya, and R. F. Smith, "RTK GPS mapping of transplanted row crops," *Comput. Electron. Agricult.*, vol. 71, no. 1, pp. 32–37, 2010.
[18] J. Kadeřábek, V. Shapoval, and P. Matějka, "Evaluation of the RTK receiver's capability of determination the accurate position," *Agronomy Res.*, vol. 16, no. 3, pp. 749–757, 2018.
[19] M. S. N. Kabir, M. Z. Song, N. S. Sung, S. O. Chung, Y. J. Kim, N. Noguchi, and S. J. Hong, "Performance comparison of single and multi-GNSS receivers under agricultural fields in Korea," *Eng. Agricult., Environ. Food*, vol. 9, no. 1, pp. 27–35, 2016.
[20] A. Marucci, A. Colantoni, I. Zambon, and G. Egidi, "Precision farming in hilly areas: The use of network RTK in GNSS technology," *Agriculture*, vol. 7, no. 7, p. 60, 2017.
[21] T. Bell, "Automatic tractor guidance using carrier-phase differential GPS," *Comput. Electron. Agricult.*, vol. 25, nos. 1–2, pp. 53–66, Jan. 2000.
[22] *FANTASTIC Project*. Accessed: Jan. 16, 2020. [Online]. Available: http://gnss-fantastic.eu/

MARCO PINI received the Ph.D. degree in electronics and communications from the Politecnico di Torino University.

He heads the Space and Navigation Technologies research area at the LINKS Foundation, Italy. As a result of the experience gained on GNSS receivers and performance, he has been responsible for the R&D activities of several projects. His major interests include the field of baseband signal processing on new GNSS signals, multifrequency RF front end design, and software radio receivers.

GIANLUCA MARUCCO received the M.S. degree in electronics engineering from the Politecnico di Torino. He is currently a Senior Researcher with LINKS Foundation, Italy, and coordinates R&D activities dealing with the application of GNSS technologies. He gained a strong experience in the test of GNSS equipment and in the collection of data in real environments; therefore, he leads the integration and validation of prototypes when these are developed by LINKS researchers as part of R&D projects.

GIANLUCA FALCO received the M.S. degree in communications engineering from the Politecnico di Torino, Italy, in 2007. Since 2011, he holds a Ph.D. degree in electronic and communication. He is currently a Communication Engineer with the Space and Navigation Technologies research area of the LINKS Foundation, Turin, Italy. His interest focuses on multisensors fusion, particularly between GPS and inertial navigation systems, as well as on advanced processing techniques for dual frequency and multiconstellation GNSS receivers.

MARIO NICOLA received the M.S. degree in computer science engineering from the Politecnico di Torino, in 2002, and the Ph.D. degree in electronics and communications engineering, in 2005, working on reconfigurable architectures for wireless communication systems.

He is currently a Researcher in the staff of the Space and Navigation Technologies research area at LINKS Foundation, Italy. His main activity is the implementation of algorithms for software radio GPS/Galileo receivers.

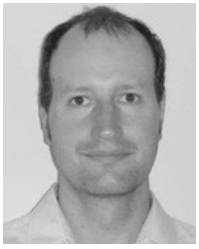

WIM DE WILDE received the M.Sc. degree in electrical engineering from the University of Ghent, in 1999. Upon graduation, he joined Alcatel Bell's research team to model and specify the first DMT VDSL integrated front-end. In 2002, he moved to Septentrio, where he created many digital IP blocks and RF frontends for GNSS and Inmarsat reception. He is currently a Systems Engineer with Septentrio. His research interests include anti-jamming and anti-spoofing techniques, multipath mitigation, and sensor fusion.